

Article

Ab Initio Study of the Combined Effects of Alloying Elements and H on Grain Boundary Cohesion in Ferritic Steels

Aparna P. A. Subramanyam [†], Abril Azócar Guzmán [†], Smobin Vincent, Alexander Hartmaier and Rebecca Janisch *

Interdisciplinary Centre for Advanced Materials Simulation, Ruhr-University Bochum, 44780 Bochum, Germany; Aparna.PuchakayalaAppiahSubramanyam@rub.de (A.P.A.S.); Abril.AzocarGuzman@rub.de (A.A.G.); smobin.vincent@rub.de (S.V.); alexander.hartmaier@rub.de (A.H.)

* Correspondence: rebecca.janisch@rub.de

† These authors contributed equally to this work.

Received: 31 January 2019; Accepted: 27 February 2019; Published: 5 March 2019



Abstract: Hydrogen enhanced decohesion is expected to play a major role in ferritic steels, especially at grain boundaries. Here, we address the effects of some common alloying elements C, V, Cr, and Mn on the H segregation behaviour and the decohesion mechanism at a $\Sigma 5(310)[001]$ 36.9° grain boundary in bcc Fe using spin polarized density functional theory calculations. We find that V, Cr, and Mn enhance grain boundary cohesion. Furthermore, all elements have an influence on the segregation energies of the interstitial elements as well as on these elements' impact on grain boundary cohesion. V slightly promotes segregation of the cohesion enhancing element C. However, none of the elements increase the cohesion enhancing effect of C and reduce the detrimental effect of H on interfacial cohesion at the same time. At an interface which is co-segregated with C, H, and a substitutional element, C and H show only weak interaction, and the highest work of separation is obtained when the substitute is Mn.

Keywords: hydrogen embrittlement; hydrogen enhanced decohesion; grain boundary embrittlement; grain boundary segregation; ab initio calculations

1. Introduction

Hydrogen being one of the most abundantly available elements is also one of the most complicated to understand. It could be the answer to the present-day energy crisis, if one could design reliable H storage materials or reduce H embrittlement (HE) of the plasma facing materials in nuclear fusion reactors. However, despite being investigated for more than 140 years [1], H embrittlement continues to be a major source of environmental degradation in structural alloys. H is a major reactant with solids because of its strong chemical activity and high lattice mobility as a result of its small size, which in turn results in high diffusivity.

The most promising approach to attempt to prevent hydrogen embrittlement is thus to influence the diffusivity of H in microstructures of iron and iron alloys [2]. Sufficiently strongly trapped hydrogen might not harm steel, as long as the accumulated hydrogen does not trigger an embrittlement mechanism of its own. For instance, grain boundaries (GBs) are likely trapping sites for H [3,4] but are also prone to suffer from hydrogen enhanced decohesion (HEDE) [5]. Both the segregation tendency of H to grain boundaries and the effect of H on GB cohesion can be influenced by alloying elements [6,7]. In the study at hand, we investigate the co-segregation of H and typical alloying elements in ferritic steels, C, V, Cr, and Mn to shed some light on their combined effects on grain boundary embrittlement. We perform

quasi-static ab initio density functional theory (DFT) calculations to obtain accurate segregation energies and mechanical quantities, which can serve as input for transport- or micromechanical models.

C is known to segregate to defects and grain boundaries due to an increased solubility at higher strain fields [8]. e.g., at dislocations, or a beneficial combination of excess volume and bond lengths at grain boundaries [9]. C also acts as a cohesion enhancing element in bcc metals [10,11]. Tahir et al. [6] investigated the physical properties of a $\Sigma 5$ symmetrical tilt GB in bcc Fe with C and H impurities through ab initio calculations, finding that C enhances the grain boundary cohesion and theoretical strength, while H does not have an important detrimental effect on its own. According to this, it can be inferred that the reason for the embrittlement is the substitution of strengthening elements, such as C, by H.

Cr has been studied in α -Fe and reported to segregate to and enhance grain boundary cohesion of $\Sigma 5(210)$ and $\Sigma 3(111)$ GBs [12,13]. The co-segregation of Cr and H was investigated in the $\Sigma 3(111)$ GB, where Cr was found to deter the segregation of H and suppress the H-induced embrittlement [7,14]. In γ -Fe, Cr is cohesion enhancing at the $\Sigma 11(11\bar{3})[1\bar{1}0]$ GB, due to strengthening chemical effects [15,16]. Similarly, V has a cohesion enhancing effect on the same $\Sigma 11$ GB [16,17]. Studies of the $\Sigma 3(111)[1\bar{1}0]$ bcc Fe GB indicated that V also has a cohesion enhancing effect [18], and, in the Fe-V-H system, it was found that there is no interaction between H and V at the GB, meaning that the presence of V does not affect the segregation of H to the grain boundary [19]. Mn alone was found to be embrittling at the $\Sigma 3(111)[1\bar{1}0]$ [20] and γ -Fe $\Sigma 11(11\bar{3})[1\bar{1}0]$ [16] GBs.

It seems that Mn is causing an increase in solubility [21,22] and mobility [21] of interstitial H in Mn-containing Fe alloys. Counts et al. [23] studied H-H interactions in the presence of 3d solute atoms in bcc Fe and found that H-solute defect complexes can contain two H atoms for Cr and V and contain four H atoms for Mn with H binding most strongly to Mn and least to Cr. A strong attraction between C and Mn was observed in bcc FeMn alloys [24] and at a $\Sigma 3(111)$ GB in bcc Fe [25] and an austenitic Fe-C-Mn alloy [26]. In this work, we confirm the C-Mn attraction in the bulk, but we find that C prefers to segregate away from Mn at the $\Sigma 5$ GB in bcc Fe. This indicates that C-Mn interaction is not necessarily the same at different GBs and in the bulk.

While the individual interactions between either H or C with typical alloying elements and the consequences for segregation and cohesion at grain boundaries have been studied in some detail, not much is known about the effect of these alloying elements on the co-segregation of H and C. State-of-the-art thermodynamic models of segregation in multicomponent systems ignore the interaction between interstitial segregants [27]. In this work, we confirm that this is a good approximation for the system Fe-X-C-H (with X = Cr, V, Mn), but that the interaction between X and the interstitial element can be significant.

This paper is structured as follows: Section 2 describes the construction of the supercell used for ab initio calculations and the procedure and formulae used in calculating the energies and mechanical properties. In Section 3, we present our findings and we discuss and conclude our work in Sections 4 and 5.

2. Methodology

2.1. Technical Details

We used the VASP software package [28–31] for the DFT calculations. The Perdew–Burke–Ernzerhof (PBE)-GGA [32] functional was used to account for the exchange and correlation effects, and the projector augmented-wave (PAW) [33] method was employed to describe the core–valence interaction. Spin-polarized calculations were performed to account for the magnetism of V, Cr, Fe and Mn. A plane-wave basis with a cut-off energy of 400 eV and an $8 \times 4 \times 2$ k-point mesh generated using the Monkhorst–Pack method [34] is used to sample the Brillouin Zone for all supercells. The convergence between a $8 \times 4 \times 2$ and $16 \times 4 \times 2$ sampling was tested for the cell_[001] supercell (see below), and the difference in solution energy of C in the presence of V was found to be less than

1 meV/atom. The convergence criteria for the electronic iteration is set to 10^{-6} eV, and the atoms are relaxed until the maximum force component on each atom is less than 10^{-2} eV/Å. The first-order Methfessel–Paxton method [35] was used for the Fermi-surface smearing with a smearing width of 0.1 eV.

2.2. Simulation Cell

We study the alloying effects at a $\Sigma 5(310)[001]$ 36.9° symmetrical tilt grain boundary (STGB) in α -Fe. To this end, a 40-atom supercell (in the following named cell_[001]) was constructed, which contains 20 (310)-layers parallel to the GB and two crystallographic planes (=one periodic unit) along the [001] tilt axis. There are two GBs due to periodic boundary conditions. This cell size allows substitution of Fe in the (310) plane in steps of 50%. To further investigate the effect of concentration of the alloying elements, case studies were carried out with an 80-atom supercell (in the following named cell_{2[001]}) of the $\Sigma 5$ STGB containing four crystallographic planes (=two periodic units) along the [001] tilt axis. This supercell size enables substitution of Fe in steps of 25% in the (310) plane. The two cells are shown in Figure 1. The cells were optimized with respect to translations parallel to and expansion perpendicular to the grain boundary, while allowing relaxations of atomic positions. For the larger cell, this was already done in a previous study [6]. The convergence with respect to the number of layers separating the two GBs was tested again in the presence of a substitutional Mn atom and found to be sufficient within an accuracy in the GB energy of 34 mJ/m^2 .

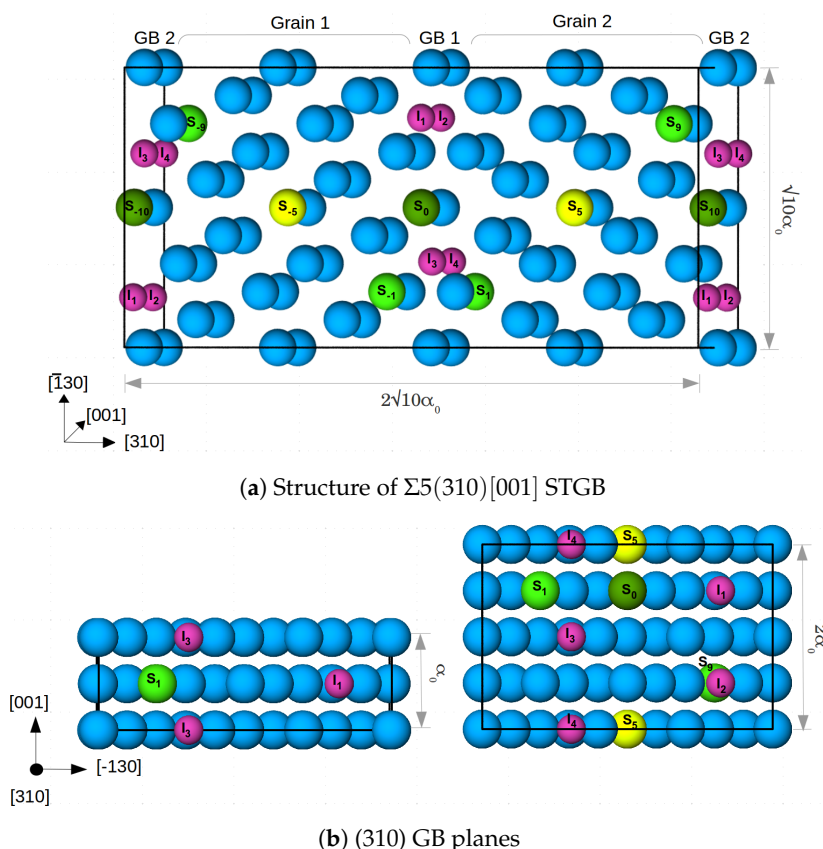


Figure 1. (a) 80 atom supercell (cell_{2[001]}) along with segregation sites for Mn, Cr and V, labelled with S and a number which marks the distance from the GB in the center (GB1). The blue colored atoms are Fe, and the segregation sites are shown in yellow (at the center of the grain), dark green at the GB and light green at the layers next to the GBs. Four segregation sites per GB for interstitial atoms—H and C (marked I₁–I₄) are also shown by small pink colored atoms. α_0 is the lattice constant of Fe; (b) the GB planes for cell_[001] (left) and cell_{2[001]} (right) along with the respective segregation sites.

Figure 1 shows the segregation sites for the alloying/impurity atoms at each GB that were considered in this study. Each alloying element is placed at each GB/in each grain to maintain the symmetry of the cell. Substitutional sites are labelled with S and a number which marks the distance from the GB in the center (GB1). Note that, in cell_[001], the atoms on positions S₁ are restricted to form columns along the [001] direction, while in the larger cell there is the option to occupy alternating or diagonally opposite sites along [−130], as shown in Figure 1b. In a previous study [9], the latter case (sites S_{−1}/S_{−9} and S₁/S₉) was found to be energetically more favourable for Mn. Thus, we added the corresponding configuration of Mn atoms in cell_{2[001]} to estimate the influence of supercell size and atomistic configuration on the segregation energy of the considered alloying elements.

I₁ to I₄ are the four segregation sites at each GB for the interstitial atoms H and C in cell_{2[001]}, while I₁ and I₃ are the two sites present in cell_[001]. These sites are in the center of capped trigonal prisms, which form the structural units (SUs) of the Σ5 (310) STGB [6,9]. In both supercells, a 100% occupation of the SUs corresponds to an area density of 0.078 C and/or H atoms per m² in the GB plane. Segregation sites I₃ and I₄ (I₁ and I₂) have a (no) substitutional alloying element at one of the corners of the trigonal prism. After determining the most likely positions for the substitutional elements (see Section 3.1.1), the most favorable segregation sites for C and H at these grain boundaries were obtained by testing all resulting nonequivalent configurations (a total of 65).

Rigid grain shifts with subsequent relaxation of the atomic positions were performed to determine the change in excess volume (expansion along [310]) and translation state along the tilt axis [001] induced by Mn, Cr and V. The results are shown in Table 1 w.r.t the pure Fe STGB. To study segregation of C and H in the presence of V, Cr or Mn, C and H were then added to the such optimized supercells with a substitutional element. These cells were further optimized by rigid grain shifts in order to account for excess volume at the GB, induced by the interstitials.

For the reference configurations in the Fe bulk, a bulk supercell with the same number of atoms and oriented in the same directions as the GB supercell was optimized in the same way.

Table 1. Effect of alloying elements on GB properties. The excess length and the shift along the tilt axis (columns five and six) are expressed with respect to the values at the pure Fe GB (first row).

System	Segregation Sites	Excess Length [Å]	Shift _[001] [Å]	γ _{GB} [J/m ²]	γ _{seg} [eV/Atom]
Fe	-	0.31	0.43	1.55	-
Fe + V	S ₀	+0.08	+0.12	1.47	−0.16
	S _{−1}	+0.06	+0.01	1.47	−0.15
Fe + Cr	S ₀	+0.09	+0.10	1.45	−0.18
	S _{−1}	+0.05	−0.03	1.40	−0.27
Fe + Mn (cell _[001])	S ₀	+0.11	−0.02	1.36	−0.33
	S _{−1}	+0.09	−0.25	1.27	−0.48
Fe + Mn (cell _{2[001]})	S ₀	+0.00	+0.00	1.59	0.12
	S _{−1}	+0.09	−0.07	1.40	−0.48
	S _{−1} , S ₁	+0.07	−0.32	1.21	−0.55

2.3. Grain Boundary and Segregation Energies

After optimization, the energy of the GB is calculated as

$$\gamma_{GB} = \frac{E_{GB}^{xFe+yS+zI} - (E_{Bulk}^{xFe+yS} + z\mu_I)}{2A}. \quad (1)$$

$E_{GB}^{xFe+yS+zI}$ is the total energy of the GB containing x Fe atoms, y substitutional atoms (Cr, V, or Mn) and z interstitial C or H atoms. E_{Bulk}^{xFe+yS} is the energy of x Fe atoms and y substitutional atoms in the bulk slab, and $z\mu_I$ is the reference energy of the z interstitial impurities: $\mu_C = −9.120$ eV/atom in the diamond phase and $\mu_H = −3.385$ eV/atom in a H₂-molecule [6].

The segregation energy of a substitutional alloying element to the GB is calculated as

$$\gamma_{seg} = E_{sol}^{GB} - E_{sol}^{Bulk} \quad , \quad (2)$$

where the solution energies per atom of substitutional alloying element S at the GB or in bulk ($E_{sol}^{GB/Bulk}$) are calculated as follows:

$$E_{sol}^{GB/Bulk} = \frac{(E_{GB/Bulk}^{xFe+yS} + y\mu_{Fe}) - (E_{GB/Bulk}^{(x+y)Fe} + y\mu_S)}{y} \quad . \quad (3)$$

$y\mu_{Fe}$ is the chemical potential of y ferromagnetic bcc Fe atoms added to conserve the number of Fe atoms, and $y\mu_S$ is the chemical potential of the same number of substitutional atoms in their respective ground states. The reference energies for the non-magnetic bcc metals are $\mu_{Cr} = -9.630$ eV/atom for Cr and $\mu_V = -9.079$ eV/atom for V, and the one for cubic, non-magnetic α -Mn is $\mu_{Mn} = -9.153$ eV/atom. The solution energy per atom of z interstitial elements at (two) Mn/Cr/V pre-segregated GBs and in the bulk alloy are defined as

$$E_{sol}^{GB/Bulk} = \frac{E_{GB/Bulk}^{(xFe+yS)+zI} - (E_{GB/Bulk}^{(xFe+yS)} + z\mu_I)}{z} \quad . \quad (4)$$

2.4. Work of Separation and Theoretical Strength

The work of separation (WoS) is the energy which is required to separate the GB into two free surfaces (FS),

$$WoS = \frac{2E_{FS} - E_{GB}}{2A} \quad , \quad (5)$$

where E_{FS} is the total energy of the FS slab with half the number of substitutional or interstitial impurity atoms (and Fe atoms) as that of GB, E_{GB} is the total energy of the GB with S and/or I . The FS slab is created by cleaving the GB supercell at the GB plane and separating GB1 and Grain2 (from Figure 1) into two free surfaces, allowing only atomic positions to relax.

The thermodynamic theory of Rice and Wang [36] relates the segregation behaviour of solutes to their effect on grain boundary cohesion. According to their model, the difference in bonding energies of a solute at a grain boundary and at the corresponding free surface is a measure of the reduction or the enhancement of cohesion that this solute causes at the interface. In other words, elements that segregate more strongly to a free surface than to the grain boundary have an embrittling effect. This can easily be seen by re-arranging the terms in the bonding energy difference to represent the difference in work of separation with and without the impurity. This difference is thus also often called strengthening energy ΔE_{SE} ,

$$\Delta E_{SE} = \frac{n}{2A} \left[\gamma_{seg}^{FS} - \gamma_{seg}^{GB} \right] = WoS^{(S/I)} - WoS^{ref} \quad , \quad (6)$$

where n is the total number of segregating atoms, y or z . A positive/negative value of ΔE_{SE} means that a solute strengthens/weakensthe GB. Note that the reference structure to calculate WoS^{ref} for substitutional elements is different from that for interstitial elements. To see the influence of the substitutional alloying elements, the WoS^{ref} is that of the pure Fe STGB, while, for the investigation of the effect of C and H, it is that of the Fe STGB with a substitutional alloying element.

To gain more insight into the nature of the cohesion enhancing/embrittling effect, we separated the change in WoS into two parts—chemical contribution ΔE_{SE}^c and mechanical contribution ΔE_{SE}^m , as described in [37,38]. ΔE_{SE}^c is the direct interaction between the solute and host atoms and is defined as the energy needed to remove the solute while not permitting the host atoms to relax. It is the

difference between the WoS of a relaxed GB structure with solute atoms and the same GB in which the solute atoms are removed without any subsequent relaxation of the atomic positions,

$$\Delta E_{SE}^c = WoS^{(S/I)} - WoS_{rigid}^{\square}. \quad (7)$$

The \square represents either the vacant interstitial site or the substitutional site now replaced by an Fe atom without further relaxation. The remaining part of ΔE_{SE} is the elastic or mechanical contribution of the host–host interaction induced by the impurity. It is characterized by the relaxation of the host metal lattice to accommodate the impurity atoms and can be obtained via

$$\Delta E_{SE}^m = WoS^{\square} - WoS_{relaxed}^{pureGB}. \quad (8)$$

Ab initio uni-axial tensile tests were performed by increasing the length along [310] via step-wise rigid separation of the two grains, where the separation between the two grains was inserted between GB2 and Grain1 and GB1 and Grain2. This type of rigid body separation requires the same force (or stress) as mode I fracture [39]. The supercells were compressed and expanded along [310] up to the free surface energy, and the universal binding energy relationship (UBER) [40] was fitted to the data. The critical stress for fracture (fracture stress σ_f) is the first derivative at the displacement at the point of inflection (where the curvature is zero) [6,39,41].

3. Results

3.1. Segregation

3.1.1. Segregation of V, Cr, and Mn to the GB

All the grain boundary and segregation energies are listed in Table 1. It can be observed that Mn decreases the GB energy and is also more strongly attracted to the GB than Cr and V. From both γ_{seg} and the decrease in γ_{GB} , we find that Cr and V at 5 at% do not show a clear preference for the GB plane or the layer next to it, while Mn has a strong preference for S₋₁. Note that, for Mn at 5 at.% in cell_{2[001]}, the energy can be further lowered by placing Mn in diagonally opposite sites S₋₁ and S₁ at GB1, and at S₋₉ and S₉ at GB2 instead of a column-wise configuration.

Both S₀ and S₋₁ sites were considered for Cr and V for all further studies with C and H. Only the site S₋₁ was considered for 2.5 at.% Mn and the sites S₋₁ / S₁ for 5 at.% Mn.

3.1.2. Segregation of C and H to the GB Segregated with V, Cr, and Mn

The grain boundary energy was calculated for different occupations of available interstitial sites by C and H atoms, using Equation (1). It can be seen in Figure 2 that the energy of the Fe STGB is reduced in the presence of C by 58–65%, depending on the substitutional alloying element (compare black and dark grey bars). H lowers the energy of the GB by 17–20%. Since the reduction of the GB energy is higher for C occupation, it can be inferred that C is more attracted to the GB than H. The substitutional atoms add to the reduction in GB energy in the presence of C and H, Mn lowering it the most in all cases. The precise values are summarized in Table A1 in Appendix A. The energies in Figure 2 represent the most favourable configurations among the different nonequivalent possibilities (see Section 2.2). In cell_[001], it was found that the solution energy of H is lower in site I₃, the SU with substitutional element in S₋₁, by 13 meV/atom for S = V, 24 meV/atom with Cr, and 29 meV/atom with Mn. C segregates to site I₃ for V in S₋₁; however, the segregation energy is lower by only 8 meV/atom than for I₁. When Cr and Mn are at S₋₁, C prefers site I₁ by 72 meV/atom and by 232 meV/atom, respectively. The grain boundary and segregation energies of C and H for a GB with 2.5 at.% Mn are shown in Figure 3. In the case of 2.5 at.% of Mn, the segregation energy for a single H or C atom (25% coverage) to the SU with Mn, i.e., site I₃, is lower by 28 meV/atom (H) and higher by

180 meV/atom (C) than for I₁. This indicates a strong preference of C for a SU of only Fe atoms instead of Cr or Mn, while H always prefers the SU with a substitutional alloying element at one of its corners.

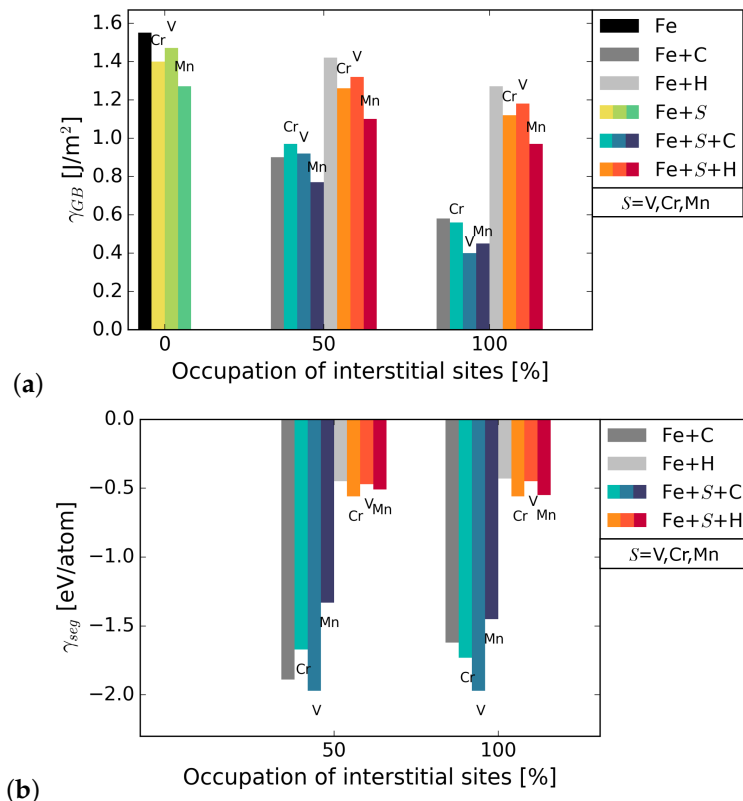


Figure 2. (a) grain boundary energy with substitutional elements S (=Cr, V, Mn) and interstitial elements C and H. The black bar on the left represents the GB energy in pure Fe. The bars in blue shades represent energies in the presence of S and C while the bars in orange shades represent energies in the presence of S and H; (b) segregation energies of the interstitial elements to the Fe STGB without (grey bars) and with substitutional element S at the boundary.

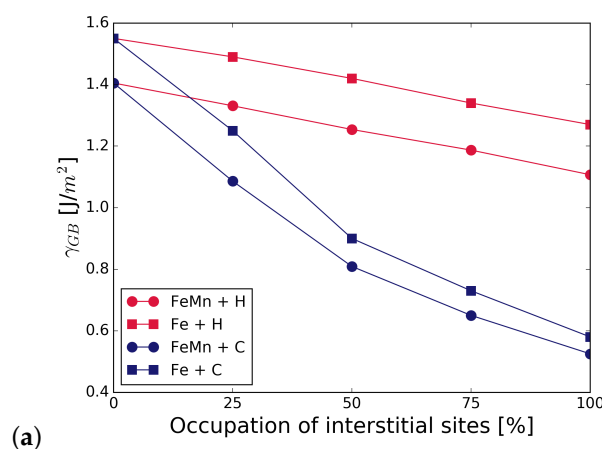


Figure 3. Cont.

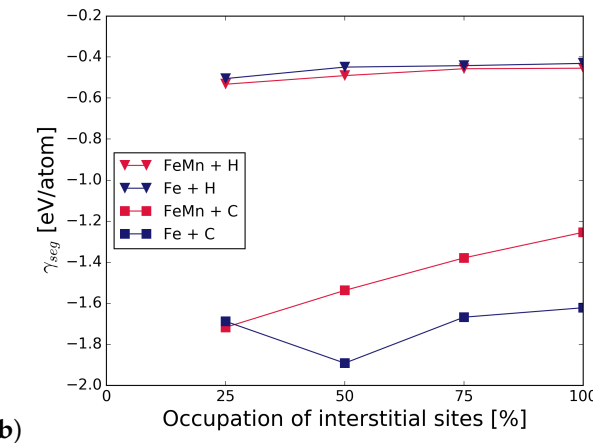


Figure 3. (a) γ_{GB} at 2.5 at.% of Mn and different occupation of the SUs with H and C; (b) effect of Mn on the γ_{seg} of H and C at 2.5 at.% of Mn.

3.1.3. Co-Segregation of C and H

Co-segregation is considered for full coverage with interstitial elements, 50% of the SUs by C and 50% of SUs by H atoms. The segregation energies were calculated according to Equation (4) and are shown in Figure 4.

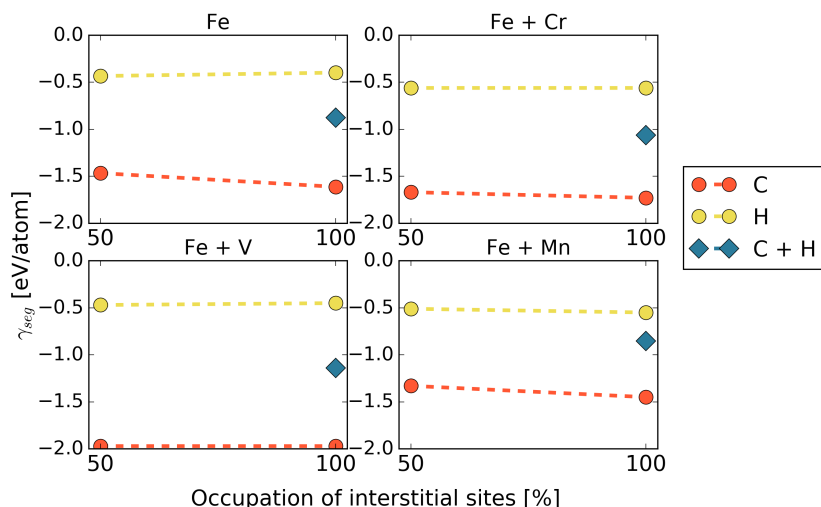


Figure 4. Segregation energies for co-segregation of C and H, in the presence of different alloying elements at the $\Sigma 5$ STGB.

In general, it is observed that co-segregation of C and H does not exhibit a lower segregation energy than that of C alone, but an average value between those of C and H. This means that, at least from a thermodynamic point of view, we always expect an excess of C at the grain boundary. Segregation of H, however, could be stronger for kinetic reasons, which are out of the scope of this study. The only exception that we found was co-segregation in the presence of Mn in $cell_{2[001]}$. Here, a combination of C and H at the grain boundary is favored in a different configuration from what would be expected from the results of C or H only (see Table 2), namely in terms of an alternating C-H arrangement along the [001] axis rather than a C-C / H-H alignment. For the higher Mn content of 5.0 at.%, this configuration has a lower segregation energy than a full occupation of the interface with either H or even C showing that the arrangement of Mn at the GB matters.

Table 2. Configuration and concentration dependence of co-segregation energies of C and H in the presence of Mn.

Structure	Occupation of SUs	Segregation Sites		γ_{seg} [eV/Atom]
		C	H	
cell _{2[001]} 2.5 at.% Mn	75%	I ₁	I ₃ , I ₄	-1.18
		I ₁ – I ₃	-	-1.38
		-	I ₁ , I ₃ , I ₄	-0.46
	100%	I ₁ , I ₃	I ₂ , I ₄	-1.18
		I ₁ – I ₄	-	-1.25
		-	I ₁ – I ₄	-0.45
cell _{2[001]} 5.0 at.% Mn	100%	I ₁ , I ₃	I ₂ , I ₄	-1.36
		I ₁ – I ₄	-	-1.08
		-	I ₁ – I ₄	-0.46
cell _[001] 5.0 at.% Mn	100%	I ₁	I ₃	-0.85
		I ₁ , I ₃	-	-1.45
		-	I ₁ , I ₃	-0.55

3.2. Mechanical Properties: Work of Separation and Fracture Stress

3.2.1. Influence of Substitutional Alloying Elements

Table 3 shows the WoS, change in strengthening energy (calculated using Equation (6)), and the chemical, ΔE_{SE}^c , and mechanical, ΔE_{SE}^m , contributions to the WoS as calculated from Equations (7) and (8), respectively, as well as the fracture stress.

Table 3. Effect of alloying elements on GB cohesion. Listed are the total work of separation (WoS), the change due to the alloying element, ΔE_{SE} , the chemical and mechanical contribution to the latter, and the fracture stress σ_f .

System	Segregation Sites	WoS [J/m ²]	ΔE_{SE} [J/m ²]	ΔE_{SE}^c [J/m ²]	ΔE_{SE}^m [J/m ²]	σ_f [GPa]
Fe		3.48				
Fe + V	S ₀	3.82	0.34	0.34	0.00	24.7
	S ₋₁	3.72	0.24	0.25	-0.01	23.6
Fe + Cr	S ₀	3.75	0.27	0.27	0.00	24.2
	S ₋₁	3.77	0.29	0.30	-0.01	23.8
Fe + Mn (cell _{1[001]})	S ₀	3.72	0.24	-0.06	0.30	23.7
	S ₋₁	3.85	0.37	0.10	0.27	24.1
Fe + Mn (cell _{2[001]})	S ₋₁	3.61	0.13	-0.20	0.33	24.6
	S ₋₁ , S ₁	3.82	0.34	0.09	0.25	26.1

All alloying elements have a positive effect on cohesion at the Σ5 GB, as can be seen in the increase in WoS, and accordingly in the positive strengthening energy ΔE_{SE} .

The chemical and mechanical contributions to the strengthening energy as seen in Table 3 show that the cohesion enhancing effect of V and Cr is more or less completely due to the chemical interaction between host and alloying element, while for Mn the mechanical contribution dominates. This is in agreement with the observation that Mn causes the largest change in the translation state of the grain boundary (see Table 1).

3.2.2. Influence of C and H on Grain Boundary Cohesion

Figure 5 summarizes the work of separation and fracture stress with and without interstitial and substitutional elements. It can be seen that there is a net cohesion enhancing effect in the presence of C and all substitutional alloying elements at all concentrations. The increase is not as substantial for C at the GB with Cr and Mn as that of C at the GB with V, or even at the pure Fe STGB (black squares). This indicates a detrimental interaction between C and Mn, and C and Cr. H generally lowers the work of separation by 10 to 15%. All substitutional elements increase this effect—the decrease in WoS follows a steeper slope. The interplay between interstitial and substitutional atoms is analyzed further by calculating the different contributions to the strengthening energy.

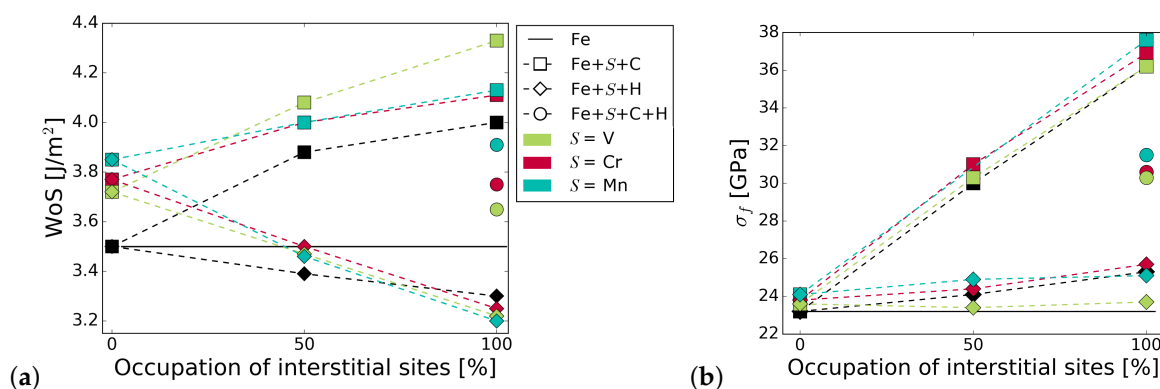


Figure 5. Effect of alloying elements on the (a) work of separation and (b) fracture strength of the GB. The x-axis represents the concentration of C or H at the GB with one of the substitutional elements $S = (\text{Cr}, \text{V}, \text{Mn})$. The black horizontal line marks the reference WoS, respectively fracture stress of the pure Fe GB. The shape of the symbols indicates the interstitial element (or the pure boundary) and the symbol color is determined by the substitutional species.

Figure 6 shows the strengthening energy divided into mechanical and chemical contributions. C has a positive chemical and mechanical contribution, where the chemical contribution clearly dominates. This is due to a re-distribution of bonding charge density into bonds across the interface [6]. For H, both contributions have a detrimental effect in the presence of all alloying elements. Mostly, it is again the chemical contribution that dominates the strengthening energy, as it can be expected for small interstitial elements.

Figure 5 also shows the mechanical properties for a 50/50 occupation of the SUs with C and H. As with the segregation energies, we find that WoS and fracture stress are the average of that in the presence of only C and only H, confirming that there is no strong interaction between H and C at the interface. Nevertheless, if the C-segregated grain boundary is considered as the reference state, such a co-segregation significantly weakens the grain boundary.

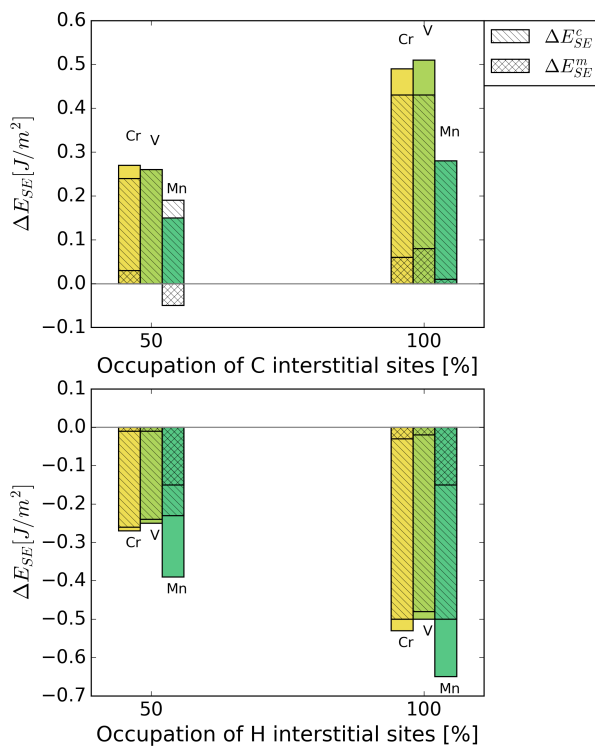


Figure 6. Mechanical (ΔE_{SE}^m) and chemical (ΔE_{SE}^c) contributions to the change in strengthening energy, ΔE_{SE} , due to the interstitial alloying elements C (top) and H (bottom).

4. Discussion

All the substitutional alloying elements, V, Cr, and Mn lower the grain boundary energy. Thus, one should expect them to be present at the $\Sigma 5$ or comparable grain boundaries. Irrespective of concentration, Mn shows the strongest tendency to segregate to the GB followed by Cr and V. All of them increase the cohesion at the GB as seen from the WoS shown in Table 3.

The interstitial elements C and H lower the grain boundary energy further from that lowered by the presence of V, Cr, and Mn. C lowers the energy approximately down to 40% of the original value of the pure Fe STGB, and H to 75%, if both elements are considered independently. This is reflected also in the strongly negative segregation energies. Judging by the segregation energies of C, Cr and Mn slightly reduce C segregation compared to the pure Fe STGB, while V is neutral. At higher concentrations, V is beneficial for C segregation. This is in agreement with the site preference of C:Step wise addition of C shows that C has a strong preference to segregate away from Mn followed by Cr, while there is a small energy gain if C segregates to the SU with V.

H weakly prefers to segregate to the SU with a substitutional alloying element in all cases. The reduction of segregation energy by the alloying elements represents an increased trapping strength of the grain boundary, thus providing a possibility to reduce the H diffusivity in steel microstructures. Unfortunately, the effect comes along with the detrimental influence of H on grain boundary cohesion, as discussed below. The site-preference of H could be due to an increase in volume and decrease in electronic density caused by V, Cr, and Mn (with a lower number of valence electrons) as H was shown to prefer sites with low electron density in bcc [3] as well as fcc Fe, where H also dissolves next to Mn, instead [21]. Mn has the largest impact on the structure of the $\Sigma 5$ STGB, increasing the excess volume and reducing the shift along the [001] axis. This changes the SU from a distorted, rather close packed one to a more regular, open trigonal prism, which then provides the most attractive environment for H. The picture changes in the case of 5 at.% Mn at the interface, if the Mn atoms are placed in segregation sites $S_{\pm 1}$. Using $cell_{[001]}$, we can probe more different configurations of H and C than in $cell_{[001]}$. In this case, the lowest energy is obtained when one of each kind of interstitial atom has an Mn

nearest neighbor, while the other is in a structural unit with only Fe at the corners. This symptom of a ternary Mn–C–H interaction deserves further attention in the future, especially since this configuration clearly promotes C–H co-segregation, as shown by the average segregation energy of -1.36 eV per atom, which is lower than the one of -1.08 eV per atom for C only.

Increasing the concentration of C increases the strength and the work of separation. This is true for the STGB with V, Cr, and Mn. The consequences, however, are less pronounced in case of Mn. When the GB is fully saturated with C, the WoS approaches that of a the Fe+C STGB without any substitutional element, but saturated with C and the additional positive effect of Mn on grain boundary cohesion is lost. The WoS is highest for the GB with C and V, although the initial increase in the WoS due to V is the lowest. The known increase in strength of the Fe STGB with increasing C concentration is not enhanced significantly by any of the substitutional alloying elements.

H reduces the work of separation in the case of V, Cr, and Mn to a lower value than it does in pure Fe. None of the elements have a significant effect on the change in fracture stress with increasing H concentration.

With a combination of H and C at the GB, WoS and fracture stress are the average of that in the presence of only C and only H (see Figure 5). This confirms that, at least at an area density of 0.078 m^{-2} , there is no interaction of C and H within the GB plane that either promotes or weakens the influence of the individual elements. This simplifies thermodynamic modelling of segregation of these light elements [27], at least for this alloy. However, the site preference shows that, in the case of additional substitutional elements in the alloy, the interaction between the interstitial and substitutional atoms has to be taken into account. The individual behaviour of C and H also has consequences for multiscale modelling of fracture along grain boundaries by means of atomistically informed continuum models. As suggested in Tahir et al. [42] and Tahir et al. [6], traction–separation laws can be derived from ab initio data, for use, e.g., in cohesive zone models [39]. In the case of H and C, the influence of the interstitial elements could be taken into account by simply scaling the peak stress and the work of separation with the concentration of the elements. Interestingly, the value for WoS and σ_f of the GB with both interstitial elements, C and H, is highest for Mn and lowest for V (at least at a C to H ratio of 1:1 at a fully covered grain boundary).

5. Conclusions

We have carried out an exemplary investigation of the combined segregation of substitutional (Cr, V, Mn) and interstitial (C) alloying elements and impurities (H) at the $\Sigma 5$ (310)[001] symmetrical tilt grain boundary (STGB) in bcc Fe to see if any of these elements promote or suppress H segregation and embrittlement. The segregation energies that were obtained can serve as input for transport or thermodynamic models to predict the elements' distribution in a steel microstructure, and the work of separation and fracture stress serve to formulate traction–separation laws for mechanical modelling of such microstructures.

Compared to pure Fe, the substitutional elements alone have a weak, but beneficial effect in the sense that they lower the grain boundary energy and increase the work of separation. Their influence on the fracture stress to cleave the grain boundary, however, is negligible.

Both C and H have negative segregation energies at the pure Fe STGB, implying that both elements segregate to the grain boundary. On average, the values of the segregation energy for C are three to four times that of H, indicating that the grain boundary should be enriched mainly with C. This leads to an increased work of separation and strength compared to the Fe grain boundary. If substitutional elements are added, V promotes C segregation by lowering its segregation energy. On the other hand, Mn lowers the segregation energy of H and increases the one of C. In both cases, the maximum change in segregation energies is around 20%; C is still predominantly attracted to the grain boundary.

If a mixture of C and H occurs, e.g., due to kinetic reasons, or due to C being bound in carbides and dislocations, the presence of C reduces the detrimental effect of H significantly. However, both the work of separation and the grain boundary strength are strongly reduced by an addition of hydrogen to

the grain boundary, if the C-segregated state is taken as reference. Concerning the influence of substitutional elements, the beneficial (detrimental) effect of V (Mn) is somewhat counterbalanced by the fact that a co-segregated GB with both C and H has the highest work of separation and fracture stress with Mn at the boundary, and the lowest with V.

Furthermore, the results for the mechanical properties of the grain boundary with co-segregated elements C and H show that there is no significant change in interaction between the two elements at the GB compared to the bulk. Thus, their effects can be treated as additive, which is advantageous for multi-scale modeling approaches. In contrast, the site-preference of the interstitial elements in the presence of the substitutional ones shows that there is an interaction of the interstitial with the substitutional elements, which should be taken into account. At least, in the case of Mn, even a three-body Mn–H–C interaction could be detected, which should be investigated by high-throughput variations of the atomic positions in even larger systems in the future.

Author Contributions: Conceptualization, A.H. and R.J.; supervision, R.J.; investigation, A.P.A.S., A.A.G. and S.V.; visualization and writing—original draft preparation, A.P.A.S. and A.A.G.; writing—review and editing, all authors.

Funding: This research received no external funding.

Acknowledgments: We acknowledge support by the German Science Foundation (DFG) Open Access Publication Funds of the Ruhr-Universität Bochum.

Conflicts of Interest: The authors declare no conflict of interest.

Appendix A. Segregation of Interstitial Elements

Table A1 summarizes the grain boundary energies and segregation energies for different area densities of either C or H at the $\Sigma 5$ STGB in Fe.

Table A1. Grain boundary (γ_{GB}) and segregation energy (γ_{seg}) of the Fe STGB with V, Cr, and Mn with different occupation of interstitial C and H atoms at the GB.

S	Segregation Site	Occupation Interstitial Sites [%]	Fe + S + C		Fe + S + C	
			γ_{GB} [J/m ²]	γ_{seg}^C [eV/Atom]	γ_{GB} [J/m ²]	γ_{seg}^H [eV/Atom]
V	S_0	50	0.92	-1.97	1.33	-0.44
		100	0.40	-1.97	1.23	-0.41
	S_1	50	0.98	-1.89	1.32	-0.47
		100	0.50	-1.89	1.18	-0.45
Cr	S_0	50	0.93	-1.67	1.33	-0.54
		100	0.53	-1.73	1.27	-0.49
	S_1	50	0.98	-1.59	1.26	-0.56
		100	0.53	-1.73	1.12	-0.56
Mn (cell _[001])	S_1	50	0.77	-1.33	1.10	-0.51
		100	0.45	-1.45	0.97	-0.55
Mn 2.5 at.% (cell _{2[001]})	S_1	25	1.09	-1.72	1.33	-0.53
		50	0.81	-1.54	1.25	-0.49
		75	0.65	-1.38	1.19	-0.46
		100	0.52	-1.25	1.10	-0.45
Mn 5 at.% (cell _{2[001]})	S_1	25	0.89	-1.66	1.13	-0.57
		100	0.49	-1.08	0.91	-0.46

References

- Johnson, W. On some remarkable changes produced in iron and steel by the action of hydrogen and acids. *Proc. R. Soc. Lond.* **1875**, *23*, 168–179. [[CrossRef](#)]
- Bhadeshia, H.K.D.H. Prevention of hydrogen embrittlement in steels. *ISIJ Int.* **2016**, *56*, 24–36. [[CrossRef](#)]

3. Du, Y.A.; Ismer, L.; Rogal, J.; Hickel, T.; Neugebauer, J.; Drautz, R. First-principles study on the interaction of H interstitials with grain boundaries in α - and γ -Fe. *Phys. Rev. B* **2011**, *84*, 144121. [[CrossRef](#)]
4. Du, Y.A.; Rogal, J.; Drautz, R. Diffusion of hydrogen within idealized grains of bcc Fe: A kinetic Monte Carlo study. *Phys. Rev. B* **2012**, *86*, 174110. [[CrossRef](#)]
5. Yamaguchi, M.; Ebihara, K.I.; Itakura, M.; Kadoyoshi, T.; Suzudo, T.; Kaburaki, H. First-principles study on the grain boundary embrittlement of metals by solute segregation: Part II. metal (Fe, Al, Cu)-hydrogen (H) systems. *Metall. Mater. Trans. A* **2011**, *42*, 330–339. [[CrossRef](#)]
6. Tahir, A.; Janisch, R.; Hartmaier, A. Hydrogen embrittlement of a carbon segregated $\Sigma 5(310)[001]$ symmetrical tilt grain boundary in α -Fe. *Mater. Sci. Eng. A* **2014**, *612*, 462–467. [[CrossRef](#)]
7. Yuasa, M.; Hakamada, M.; Chino, Y.; Mabuchi, M. First-principles study of hydrogen-induced embrittlement in Fe grain boundary with Cr segregation. *ISIJ Int.* **2015**, *55*, 1131–1134. [[CrossRef](#)]
8. Hristova, E.; Janisch, R.; Drautz, R.; Hartmaier, A. Solubility of carbon in α -iron under volumetric strain and close to the $\Sigma 5(310)[001]$ grain boundary: Comparison of DFT and empirical potential methods. *Comput. Mater. Sci.* **2011**, *50*, 1088–1096. [[CrossRef](#)]
9. Wang, J.; Janisch, R.; Madsen, G.K.; Drautz, R. First-principles study of carbon segregation in bcc iron symmetrical tilt grain boundaries. *Acta Mater.* **2016**, *115*, 259–268. [[CrossRef](#)]
10. Kurishita, H.; Oishi, A.; Kubo, H.; Yoshinaga, H. Grain boundary fracture in molybdenum bicrystals with various $<110>$ symmetric tilt boundaries. *Trans. Jpn. Inst. Met.* **1985**, *26*, 341–352. [[CrossRef](#)]
11. Wu, R.; Freeman, A.J.; Olson, G.B. Effects of carbon on Fe-grain-boundary cohesion: First-principles determination. *Phys. Rev. B* **1996**, *53*, 7504–7509. [[CrossRef](#)]
12. Wachowicz, E.; Ossowski, T.; Kiejna, A. Cohesive and magnetic properties of grain boundaries in bcc Fe with Cr additions. *Phys. Rev. B* **2010**, *81*, 094104. [[CrossRef](#)]
13. Shang, J.X.; Zhao, X.D.; Wang, F.H.; Wang, C.Y.; Xu, H.B. Effects of Co and Cr on bcc Fe grain boundaries cohesion from first-principles study. *Comput. Mater. Sci.* **2006**, *38*, 217–222. [[CrossRef](#)]
14. He, B.; Xiao, W.; Hao, W.; Tian, Z. First-principles investigation into the effect of Cr on the segregation of multi-H at the Fe $\Sigma 3$ (111) grain boundary. *J. Nucl. Mater.* **2013**, *441*, 301–305. [[CrossRef](#)]
15. Yang, R.; Wang, Y.M.; Ye, H.Q.; Wang, C.Y. Effects of Cr, Mn on the cohesion of the γ -iron grain boundary. *J. Phys. Condens. Matter* **2001**, *13*, 4485–4493. [[CrossRef](#)]
16. Yang, R.; Huang, R.Z.; Wang, Y.M.; Ye, H.Q.; Wang, C.Y. The effects of 3d alloying elements on grain boundary cohesion in gamma-iron: A first principles study on interface embrittlement due to the segregation. *J. Phys. Condens. Matter* **2003**, *15*, 8339–8349. [[CrossRef](#)]
17. Shang, J.X.; Wang, C.Y.; Zhao, D.L. First-principles investigation of the effect of alloying elements Ti, V on grain boundary cohesion of FCC Fe. *Comput. Mater. Sci.* **2001**, *22*, 193–199. [[CrossRef](#)]
18. Shang, J.X.; Wang, C.Y. Electronic effects of alloying elements Nb and V on body-centred-cubic Fe grain boundary cohesion. *J. Phys. Condens. Matter* **2001**, *13*, 9635–9644. [[CrossRef](#)]
19. Tian, Z.X.; Yan, J.X.; Hao, W.; Xiao, W. Effect of alloying additions on the hydrogen-induced grain boundary embrittlement in iron. *J. Phys. Condens. Matter* **2011**, *23*, 015501. [[CrossRef](#)] [[PubMed](#)]
20. Zhong, L.; Wu, R.; Freeman, A.J.; Olson, G.B. Effects of Mn additions on the P embrittlement of the Fe grain boundary. *Phys. Rev. B* **1997**, *55*, 11133–11137. [[CrossRef](#)]
21. Ismer, L.; Hickel, T.; Neugebauer, J. Ab initio study of the solubility and kinetics of hydrogen in austenitic high Mn steels. *Phys. Rev. B* **2010**, *81*, 094111. [[CrossRef](#)]
22. von Appen, J.; Dronskowski, R.; Chakrabarty, A.; Hikel, T.; Spatschek, R.; Neugebauer, J. Impact of Mn on the solution enthalpy of hydrogen in austenitic Fe-Mn alloys: A first-principles study. *J. Comput. Chem.* **2014**, *35*, 2239–2244. [[CrossRef](#)] [[PubMed](#)]
23. Counts, W.; Wolverton, C.; Gibala, R. First-principles energetics of hydrogen traps in α -Fe: Point defects. *Acta Mater.* **2010**, *58*, 4730–4741. [[CrossRef](#)]
24. Medvedeva, N.I.; Van Aken, D.C.; Medvedeva, J.E. The effect of carbon distribution on the manganese magnetic moment in bcc Fe-Mn alloy. *J. Phys. Condens. Matter* **2011**, *23*, 326003. [[CrossRef](#)] [[PubMed](#)]
25. Wicaksono, A.T.; Militzer, M. Interaction of C and Mn in a $\Sigma 3$ grain boundary of bcc iron. *IOP Conf. Ser. Mater. Sci. Eng.* **2017**, *219*, 012044. [[CrossRef](#)]
26. Enomoto, M.; White, C.L.; Aaronson, H.I. Evaluation of the effects of segregation on austenite grain-boundary energy in Fe-C-X alloys. *Metall. Mater. Trans. A* **1988**, *19*, 1807–1818. [[CrossRef](#)]

27. Scheiber, D.; Romaner, L.; Fischer, F.; Svoboda, J. Kinetics of grain boundary segregation in multicomponent systems—The example of a Mo-C-B-O system. *Scr. Mater.* **2018**, *150*, 110–114. [[CrossRef](#)]
28. Kresse, G.; Hafner, J. Ab initio molecular dynamics for liquid metals. *Phys. Rev. B* **1993**, *47*, 558–561. [[CrossRef](#)]
29. Kresse, G.; Hafner, J. Ab initio molecular-dynamics simulation of the liquid-metal–amorphous-semiconductor transition in germanium. *Phys. Rev. B* **1994**, *49*, 14251–14269. [[CrossRef](#)]
30. Kresse, G.; Furthmüller, J. Efficiency of ab initio total energy calculations for metals and semiconductors using a plane-wave basis set. *Comput. Mater. Sci.* **1996**, *6*, 15–50. [[CrossRef](#)]
31. Kresse, G.; Furthmüller, J. Efficient iterative schemes for ab initio total-energy calculations using a plane-wave basis set. *Phys. Rev. B* **1996**, *54*, 11169–11186. [[CrossRef](#)]
32. Perdew, J.P.; Burke, K.; Ernzerhof, M. Generalized gradient approximation made simple. *Phys. Rev. Lett.* **1996**, *77*, 3865–3868. [[CrossRef](#)] [[PubMed](#)]
33. Blöchl, P.E. Projector augmented-wave method. *Phys. Rev. B* **1994**, *50*, 17953–17979. [[CrossRef](#)]
34. Monkhorst, H.J.; Pack, J.D. Special points for Brillouin-zone integrations. *Phys. Rev. B* **1976**, *13*, 5188–5192. [[CrossRef](#)]
35. Methfessel, M.; Paxton, A.T. High-precision sampling for Brillouin-zone integration in metals. *Phys. Rev. B* **1989**, *40*, 3616–3621. [[CrossRef](#)]
36. Rice, J.R.; Wang, J.S. Embrittlement of interfaces by solute segregation. *Mater. Sci. Eng. A* **1989**, *107*, 23–40. [[CrossRef](#)]
37. Geng, W.T.; Freeman, A.J.; Wu, R.; Geller, C.B.; Raynolds, J.E. Embrittling and strengthening effects of hydrogen, boron, and phosphorus on a $\Sigma 5$ nickel grain boundary. *Phys. Rev. B* **1999**, *60*, 7149–7155. [[CrossRef](#)]
38. Janisch, R.; Elsässer, C. Segregated light elements at grain boundaries in niobium and molybdenum. *Phys. Rev. B* **2003**, *67*, 224101. [[CrossRef](#)]
39. Möller, J.J.; Bitzek, E.; Janisch, R.; ul Hassan, H.; Hartmaier, A. Fracture ab initio: A force-based scaling law for atomistically informed continuum models. *J. Mater. Res.* **2018**, *33*, 3750–3761. [[CrossRef](#)]
40. Rose, J.H.; Smith, J.R.; Guinea, F.; Ferrante, J. Universal features of the equation of state of metals. *Phys. Rev. B* **1984**, *29*, 2963–2969. [[CrossRef](#)]
41. Janisch, R.; Ahmed, N.; Hartmaier, A. Ab initio tensile tests of Al bulk crystals and grain boundaries: Universality of mechanical behavior. *Phys. Rev. B* **2010**, *81*, 184108. [[CrossRef](#)]
42. Tahir, A.M.; Janisch, R.; Hartmaier, A. Ab initio calculation of traction separation laws for a grain boundary in molybdenum with segregated C impurities. *Model. Simul. Mater. Sci. Eng.* **2013**, *21*, 075005. [[CrossRef](#)]



© 2019 by the authors. Licensee MDPI, Basel, Switzerland. This article is an open access article distributed under the terms and conditions of the Creative Commons Attribution (CC BY) license (<http://creativecommons.org/licenses/by/4.0/>).